Effect of retrogression re-aging treatment on corrosion behavior of 7055 Al-Zn-Mg alloy

Fuqiang Guo [a], Shuwei Duan [a], Dongting Wu [b], Kenji Matsuda [c], Tao Wang [a], Yong Zou [d*]**

a. School of Materials Science and Engineering, Shandong University, Jinan 250061, China
b. Key Laboratory of Liquid-Solid Structural Evolution and Processing of Materials, Ministry of Education, Shandong University, Jinan, 250061, China
c. Faculty of Sustainable Design, University of Toyama, Toyama 930-8555, Japan
d. Shandong Engineering & Technology Research Center for Modern Welding, Shandong University, Jinan, 250061, China

Abstract: The effect of retrogression re-aging treatment (RRA) on corrosion behavior of 7055 Al-Zn-Mg alloy were studied. Results provides the corrosion resistance could be greatly improved by RRA. After the RRA treatment, the isolated precipitates occurred on grain boundaries (GBs) and the low angle grain boundaries (LAGBs) presented a larger fraction compared to the single-stage peaking aging. The samples after RRA treatment also show better corrosion resistance than the single-stage peak aging. The results of electrochemical impedance spectroscopy (EIS) show that impedance spectrum is consisted of semi-infinite layer diffusion impedance and stagnant Weber impedance. The semi-infinite layer diffusion impedance corresponded a limited retention layer on the electrode surface. In corrosion process, Weber impedance corresponded to stagnant layer of corrosion products generated by the anode branches. The RRA sample has the high Rf and low Cf, Cp values, and the corrosion current density of the RRA samples is ten times less than the single-stage peak aging samples with the 10% hardness losing.

Keywords: Al-Zn-Mg alloy; Retrogression re-aging treatment; Corrosion; Electrochemistry

1 Introduction

For the automotive and aerospace industries, a 10% reduction in weight will bring an 8% increase in the fuel economy of automobiles. Therefore, the structural components of lightweight aluminum alloy have become the preferred materials in today's transportation industry[1]. Al-Zn-Mg alloy is widely used in the field of aerospace due to its high-strength, low density, high hardness and good machining property.

At present, many heat treatment methods were studied to enhance the performances of the aluminum alloy, including single-stage aging (T6), double-stage aging and retrogression re-aging treatment, etc. Single-stage aging treatment is performed at a single temperature for a certain period. Temperature and aging time have great influence on the microstructure and properties of aluminum alloy. The precipitation of strengthening phase in Al-Mg-Zn aluminum alloy can be separated out in a certain sequence: Supersaturated solid solution (SSSS) → Guinier → Preston (G.P) zones Metastable η` →Stable η($MgZn_2$) [2]. The 7 series aluminum alloy have higher strength after T6 treatment than that of by other heat treatments, this can be attributed that the precipitates have high density in matrix after the T6 treatment. However, the continuous coarser chain-like precipitates are distributed in the grain boundary after peak aging, these continuous grain boundary precipitates are very sensitive to the stress corrosion (SCC) and exfoliation corrosion. Retrogression re-aging treatment (RRA) can improve its SCC resistance with slightly losing the strength or plasticity, this can be attributed to the discontinuous precipitates at grain boundaries. The influence of heterogeneous precipitation is complicated in 7xxx alloy, metastable G.P zones plays an important role in precipitation kinetics [3]; η′ and η phase ($MgZn_2$) precipitate on grain interior and grain boundary together, such microstructure results the RRA samples

* Corresponding author. Tel: +86-531-88399872
E-mail: yzou@sdu.edu.cn (Yong Zou) or wxm689wxm@sdu.edu.cn (Tao Wang),

Preprints (www.preprints.org) | NOT PEER-REVIEWED | Posted: 9 July 2020 doi:10.20944/preprints202007.0173.v1

could obtain both corrosion resistance and mechanical strength [4], it has been suggested that the main micro-mechanism to achieve a good balance between strength and corrosion resistance is due to ensure the enough G.P zones in the pre-aging stage and make η′ phases dissolve in the retrogression stage and precipitate sufficiently during re-aging. In addition, enough time is necessary for Cu to diffuse from the matrix to precipitates during the slow heating process [5]。

In recent years, there are many researches on the heat treatment of 7xxx aluminum aimed to improving the performance of the alloys, especially in terms of strength and corrosion resistance. Chen et al. [6] showed that high strength, toughness and ductility been obtained of 7055 alloy after two-stage solution treatment, peak aging treatment can improve the strength of the alloy, but grain boundaries with continuous η phase after peak aging treatment are the susceptive anode channel, and the continuous η phase offers a path for inter-granular corrosion [7]; Lin et al. [8] found that the samples treated by RRA treatment have better tensile strength than that treated by the peak aging and over-aging treatments, but the samples treated by peak aging treatment have better stress corrosion resistance than that treated by RRA and over-aging treatments. Zhang et al. [9] showed that the 3D exfoliation corrosion morphology and cross-sectional morphology in peak-aged Al 7075 had obvious difference under various solid solution conditions, after the exfoliation corrosion test, a large number of corrosion pits appeared on the surface. The corrosion resistance of 7 series alloys can be obviously improved through changing single-stage peak aging (T6) treatment to retrogression re-aging (RRA) treatment, therefore, RRA is an important method to improve the corrosion resistance of 7 series aluminum alloys without significant loss of the strength.

Moreover, many researchers found that the characteristics of grains also affected the final corrosion resistance of aluminum alloy. Such as Amjad Saleh El-Amoush [10] discovered that grain coarsening at single-stage aging could reduce the breakdown potential in degassed NaCl solution，Huang et al.[11] found that the corrosion morphology is related to the grain size of T6 treated aluminum alloy. Therefore, it is very necessary to understand the influence mechanism of heat treatment process on properties of 7xxx aluminum alloy.

The present researches mainly focused on the balance between high strength and corrosion resistance of 7055 alloy, it is difficult to prepare aluminum alloy with both high-strength and high corrosion resistance property [12]. In this research, the influence of retrogression re-aging treatment and single-stage aging treatment on microstructure and corrosion behavior of 7055 alloy were systematically studied, and the corrosion mechanism was further discussed.

2. Materials and Methods

2.1 Materials and heat treatment

The experimental material is rolled commercial 7055 aluminum alloy. Its chemical composition is shown in Table 1.

Table1 The chemical composition of the 7055Al

Element	Zn	Mg	Cu	Mn	Si	Ti	Fe	Zr	Al
wt.%	7.745	1.824	2.130	0.002	0.092	0.100	0.110	0.085	Bal.

The samples was cut by electric spark from rolled plate，both single-stage aging and retrogression re-aging simples were first treated by solution treatment at 485°C for 8 h, followed by quenched in water at room temperature. Then the aging treatments were carried out. The aging parameters are listed in Table 2 and Table 3:

Table 2 Single-stage aging heat treatment parameters

Sample number	Aging temperature	Aging time
D1	120 °C	4 h
D2	120 °C	8 h

Preprints (www.preprints.org) | NOT PEER-REVIEWED | Posted: 9 July 2020 doi:10.20944/preprints202007.0173.v1

D3	120 °C	10 h
D4	120 °C	12 h
D5	130 °C	4 h
D6	130 °C	8 h
D7	130 °C	10 h
D8	130 °C	12 h
D9	140 °C	4 h
D10	140 °C	8 h
D11	140 °C	10 h
D12	140 °C	12 h

Table 3 Retrogression re-aging heat treatment parameters

Sample number	Pre-aging	Retrogression	Re-prescription
RRA1	120 °C /8 h	170°C /30 min	120 °C /24 h
RRA2	120°C /8 h	170°C /1 h	120°C /24 h
RRA 3	120 °C /8 h	170 °C /2 h	120°C /24 h
RRA 4	120°C /8 h	190°C /30 min	120°C /24 h
RRA 5	120 °C /8 h	190°C /1 h	120°C /24 h
RRA 6	120°C /8 h	190°C /2 h	120°C /24 h
RRA 7	120°C /24 h	190°C /30 min	120°C /24 h
RRA 8	120 °C /24 h	190 °C /1 h	120°C /24 h
RRA 9	120 °C 24 h	190°C /2 h	120°C /24 h

2.2 Hardness Test

The Vickers hardness of the samples were measured on a DHV-1000 digital hardness tester under a load of 100 g and a holding time of 15 s.

2.3 Intergranular corrosion test

Intergranular corrosion tests were carried out on the samples with peak aging parameters and some retrogression re-aging parameters. The samples after heat treatment were sanded to 3000 meshes and soaked into the corrosive aqueous solution of 57g/L NaCl+10ml/L H2O2 (ISO 11846-1995) for 6 hours with the same area [13]. Next, the samples were cleaned with concentrated nitric acid and ultrasonic. Scanning observation and laser confocal scanning microscope roughness tests were performed by the LSM-800 Carl Zeiss (Shanghai) Co., Ltd, intergranular corrosion levels of the samples with different heat treatments were decided by the corrosion depth.

2.4 Electrochemical test

The samples were sanded to 3000 meshes with sandpaper, wiped with alcohol, then electrochemical measurement, polarization scanning and electrochemical impedance spectroscopy were prepared in a conventional standard electrolytic cell. In the cell, the samples were the working electrode, a platinum foil as the auxiliary electrode, and a saturated calomel electrode (SCE) was the reference electrode. Electrolyte solution of 3.5% NaCl was used. The analysis was carried out with CHI660e electrochemical workstation of Shanghai Chenhua Instrument Co., Ltd, using a three-electrode system, the working face of the sample is 15 mm×10 mm×5mm. Then open circuit potential was determined by the open circuit potential-time curve test. The polarization curve was tested by potentiodynamic scanning method, and the scanning frequency of polarization curve was 0.001 V/s. Electrochemical impedance spectroscopy test used AC sine wave with amplitude of 10 mV as excitation

Preprints (www.preprints.org) | NOT PEER-REVIEWED | Posted: 9 July 2020 doi:10.20944/preprints202007.0173.v1

signal and frequency range of 0.01~105 Hz. ZView2 software was used to fit the impedance spectrum data.

2.5 X-ray diffraction (XRD)

X-ray diffraction (XRD) patterns were obtained by using an DX—2700 X-ray diffractometer at a scanning rate of 0.02°/s.

2.6 Electron backscattered diffraction (EBSD)

EBSD samples were prepared using electrolytic polishing. We used a JSM-7800F scanning electron microscope (SEM) (Tokyo, Japan) and Oxford NordlysMax3 system to acquire EBSD data, and then processed them with Channel 5 commercial software (v5.12.67.0).

2.7 Transmission electron microscope (TEM)

The samples were mechanically thinned to 120 μm. Thin foils with diameter of 3 mm were punched from the slices and then electro-polished to 30 μm. Finally, twin-jet thinning was conducted and TEM samples were obtained. TEM micrographs, including selected area diffraction (SAD) and bright-field (BF) images were taken with EM-002B operated at 120 kV.

3. Results

3.1 Hardness and the polarization curves

Fig. 1 are the results of hardness test for the samples treated by different parameters. Fig. 1(a) indicates the relationship between the hardness and single-stage aging time. Figure 1.b indicates the relationship between the hardness and time of RRA aging retrogression. It can be seen that sample of D6 (130 °C /8 h) has the highest hardness, while sample of RRA6 (120 °C /8h + 190 °C /2h + 120 °C/24h) has the lowest hardness.

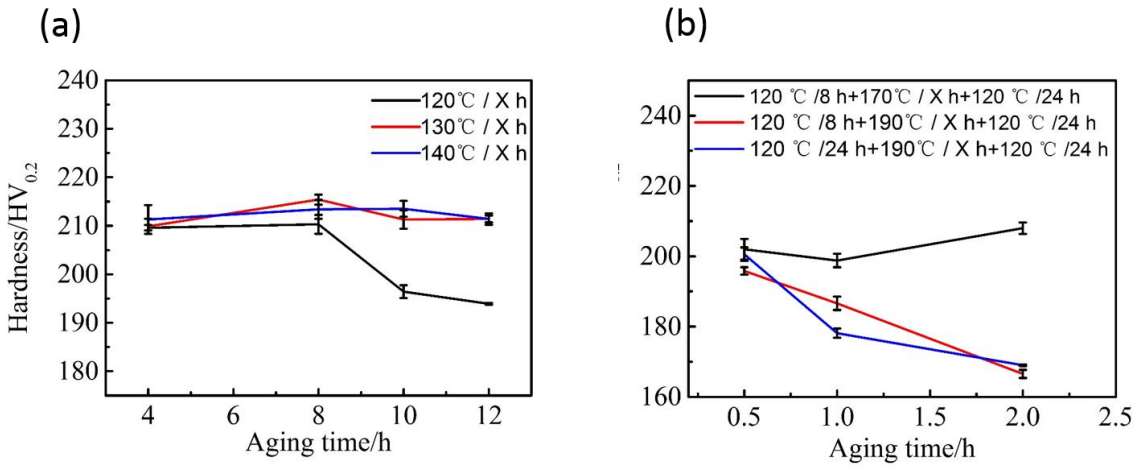

Fig.1. Hardness of (a) single-stage aging and (b) retrogression re-aging treatment

3.2 The polarization curves

The potentiodynamic polarization curves of single-stage aging D2, D6, D11 and retrogression re-aging RRA2, RRA3, RRA4, RRA6, RRA7, RRA9 parameter samples immersed in 3.5% NaCl solution is presented in Fig.2. It is found that the curves of all samples form a current platform, and the current platform of RRA samples is more obvious than T6 samples. The cathode branch is attributed to the hydrogen evolution reaction, the anode branch is related to the dissolution of the aluminum matrix, which is attribute to the transformation of aluminum ions [9, 14]. The corrosion current density is displayed in table 4. According to the corrosion current density, the corrosion resistance order of the

Preprints (www.preprints.org) | NOT PEER-REVIEWED | Posted: 9 July 2020 doi:10.20944/preprints202007.0173.v1

samples is RRA 6 > RRA 9 > RRA 7 >RRA 4 > RRA 2 > RRA 3 > D 11 > D 2 > D 6. All T6 samples showed poor corrosion resistance than that of RRA samples, among which D6 sample showed the lowest corrosion resistance and RRA6 parameter sample showed the highest corrosion resistance. According to the corrosion current density, the corrosion resistance order of the RRA samples is RRA 2 > RRA 3, RRA 6 > RRA 4, RRA 9 > RRA 7. Through the electrochemical tests, RRA 2,6,9 samples with good corrosion resistance were selected for the subsequent study.

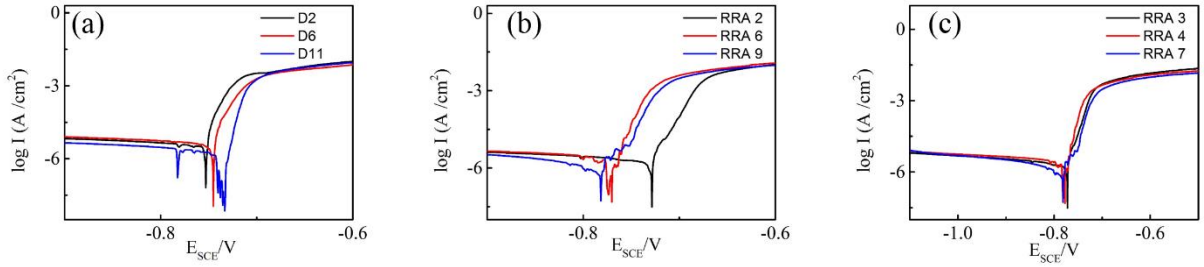

Fig. 2. Potentiodynamic polarization curves: (a) the D 2, D 6 and the D 11 samples; (b) the RRA 2, RRA 6 and the RRA 9 samples; (c) the RRA 3, RRA 4 and the RRA 7 samples.

Table 4 Corrosion potential and corrosion current density

Sample number	corrosion current density (A/cm2)
D2	3.04 E-6
D6	5.48 E-6
D11	2.58 E-6
RRA 2	1.62 E-6
RRA 3	3.08 E-6
RRA 4	8.08 E-7
RRA 6	4.28 E-7
RRA 7	6.98 E-7
RRA 9	6.59E-7

3.3 Intergranular corrosion

The influence of corrosion on degrees of roughness was analyzed by laser confocal microscopy. Fig.3 displays the typical corroded surface scanning pictures of simples of single-stage aged D2, D6, D11 and retrogression re-aged RRA2, RRA6, RRA9. Fig.4 indicates the corresponding roughness photos. As presented in Fig. 3 and Fig. 4, intergranular corrosion occurred in all samples and a large number of corrosion pits were found in both grain interior and grain boundaries. However, the pitting corrosion on the samples treated by retrogression re-aging are slightly, the samples of T6 state were more susceptible to pitting corrosion than RRA. As presented in fig. 3, D6 sample occurred more corrosion attack than samples treated by other treatments, it also showed large pitting pits, deep intergranular corrosion, and a large number of corrosion products on the surface, which indicates that it has the lower corrosion resistance than samples treated by other treatments. Retrogression re-aging samples showed better corrosion resistance, only slight pitting attacks were apperceived on their surface.

Preprints (www.preprints.org) | NOT PEER-REVIEWED | Posted: 9 July 2020 doi:10.20944/preprints202007.0173.v1

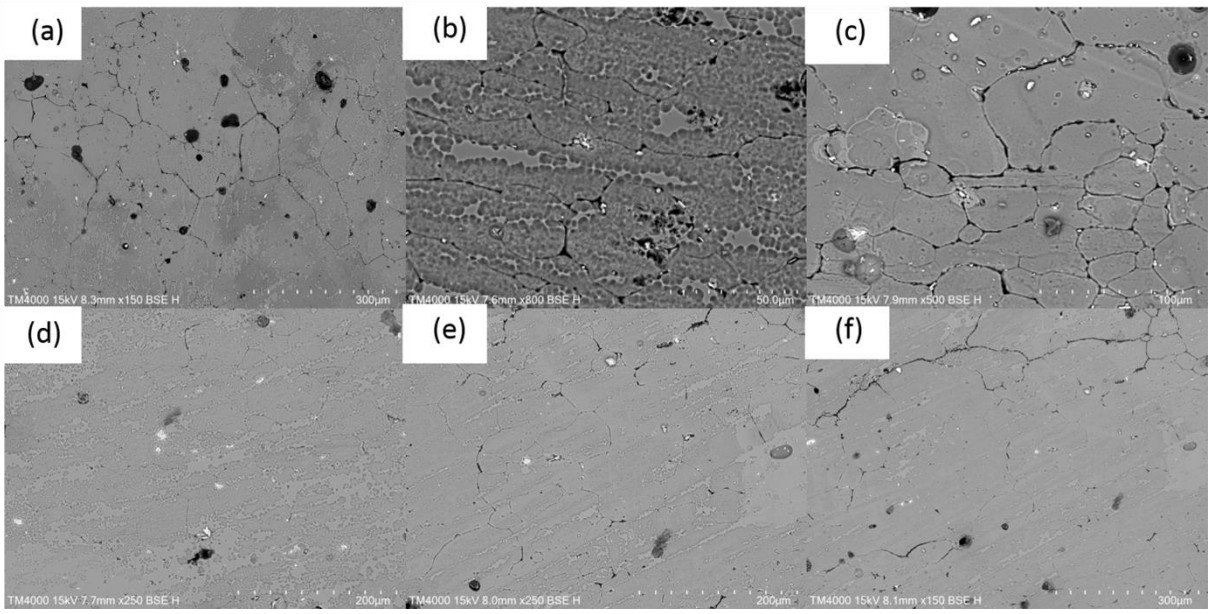

Fig.3. Corrosion metallographic photograph: (a) the D2 sample; (b) the D6sample; (c) the D11 sample; (d) the RRA2 sample; (e) the RRA6 sample; (f) the RRA9 sample.

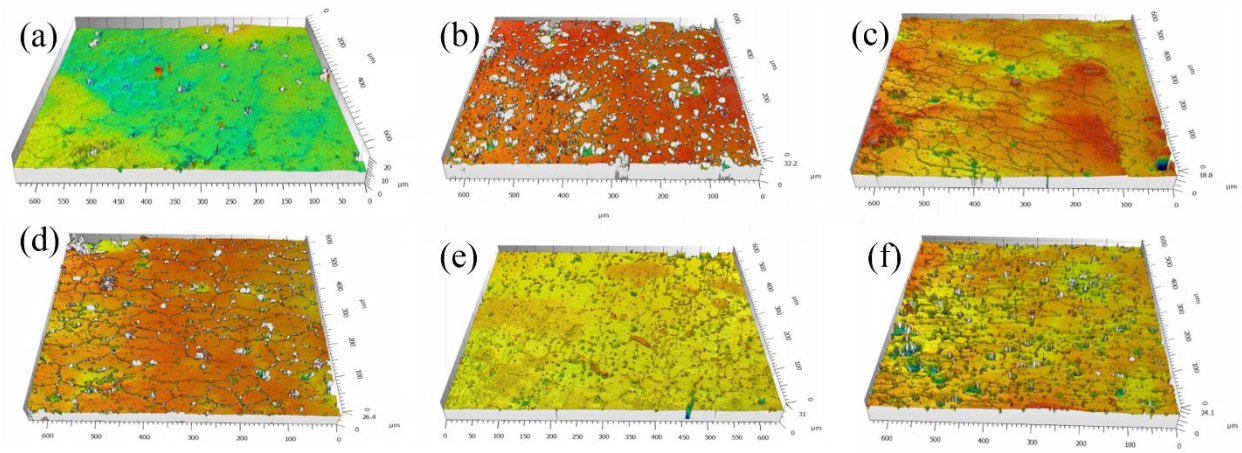

Fig. 4. The corresponding roughness photograph: (a) the D 2 sample; (b) the D 6sample; (c) the D 11 sample; (d) the RRA 2 sample; (e) the RRA6 sample; (f) the RRA9 sample

Preprints (www.preprints.org) | NOT PEER-REVIEWED | Posted: 9 July 2020 doi:10.20944/preprints202007.0173.v1

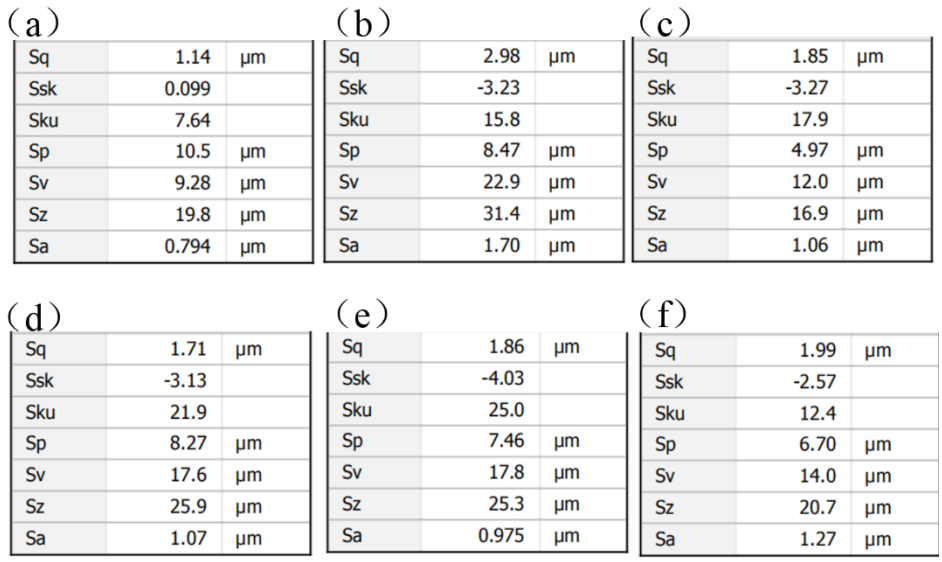

Fig. 5. The corresponding roughness values: (a) the D 2 sample; (b) the D 6sample; (c) the D 11 sample; (d) the RRA 2 sample; (e) the RRA6 sample; (f) the RRA9 sample.

As presented in Fig. 5, the average arithmetic height of D6 samples is 1.70um, and this value is 0.975um of RRA6 samples, which indicates that the average roughness of corrosion samples after RRA6 aging is lower than the d6 samples. The average root mean square height of the D6 sample is 2.98um, and the average root mean square height of the RRA6sample is 1.86um, which indicates that the standard deviation of the average height of the RRA6 corrosion samples is lower than that of the D6 corrosion samples, so the RRA6 samples have higher corrosion resistance than other samples. According to the study of grain size, grain coarsening of seven-series aluminum alloy results in the decreasing corrosion resistance [10]. However, in general, the corrosion depth of RRA samples is shallower than that of T6 samples. As indicated in the table 5, only D6 sample has an intergranular corrosion level of 3, which proves the D6 sample has the lower corrosion resistance than the samples treated by other treatments.

Table 5 Intergranular corrosion levels of the samples with different heat treatments

Sample number	Maximum corrosion depth（um）	Intergranular corrosion level
D2	19.8	2
D6	31.4	3
D11	16.9	2
RRA2	25.9	2
RRA6	20.3	2
RRA9	20.7	2

3.4 The Impedance spectrum

The impedance spectrum pictures of samples are presented in Fig.6. It can be seen that the impedance spectrum conforms to semi-infinite diffusion type. The low frequency band of the impedance spectrum develops the trend of a straight line, and the high frequency band arc can be understood as electrochemical polarization capacitance. The straight line is electrode reaction controlled by diffusion. During electrochemical corrosion process, the corrosion products were generated in anode branch, which affects the flowing of corrosion liquid, and formed a stagnant layer with a thin thickness. As a result, the low frequency band of the impedance spectrum has tendency of a straight line and a semi-infinite diffusion. An equivalent circuit diagram of the corresponding to impedance spectrum data

Preprints (www.preprints.org) | NOT PEER-REVIEWED | Posted: 9 July 2020 doi:10.20944/preprints202007.0173.v1

is presented in Fig.6. The resistance and capacitance are changed until the predicted alternate current behavior is as close as possible to the corrosion experimental data. The physical meaning of equivalent circuit elements is as follows: Rs is the ohmic resistance of electrolyte, R_f is the film resistance, C_f is the film capacitance, R_f is the hole resistance of film, C_p is the capacitance of aluminum alloy double layer, R_p is the polarization resistance of electrode, and W is Weber impedance. In this equivalent circuit, all capacitors are modeled by constant phase element (CPE) to obtain better simulation results between the model and experimental data. Then it defined by the following equation:

$$Z_{CPE} = \frac{Z_0}{(j\omega)^n}$$

Where n can be between 0 and 1 (for a perfect capacitor) and Z0 is a constant [15, 16]。 The electrochemical impedance data of its equivalent circuit elements are displayed in Table 6. It is found that all samples have similar Rs values. Due to the dissolution of aluminum and the formation of protective oxide, all samples have larger R_f values, indicating that the corrosion process is slowly, and the increasing of oxide layer thickness is attributed to the decreasing of interfacial capacitance [17]. The D2 sample has larger R_f resistance value and smaller C_p capacitance value than other samples, which indicates the oxide layer has the larger thickness and higher corrosion resistance than the D6 and D11 samples. The R_f resistance value of all RRA samples is larger than that of T6 samples, and the C_f capacitance is smaller than that of T6 samples, indicating that the RRA samples have larger oxide layer thickness and higher corrosion resistance than that of T6 samples. The system involves film formation, so the systems are not easy to polarization and have good corrosion resistance due to the high R_f, R_p and low C_f, C_p. Similarly, the D6 sample is more vulnerable to corrode and has the lower corrosion resistance than other samples. RRA6 sample has the high R_f and low C_f, C_p values, so it has better polarization and corrosion resistance than other samples. This conclusion is consistent with the above conclusions of corrosion current density and roughness test. From the above results, it can be seen that the T6 and RRA samples have the same corrosion mechanism, but the samples shows obvious difference in impedance spectrum due to the change of surface corrosion oxide thickness caused by the differences of precipitation quantity and distribution.

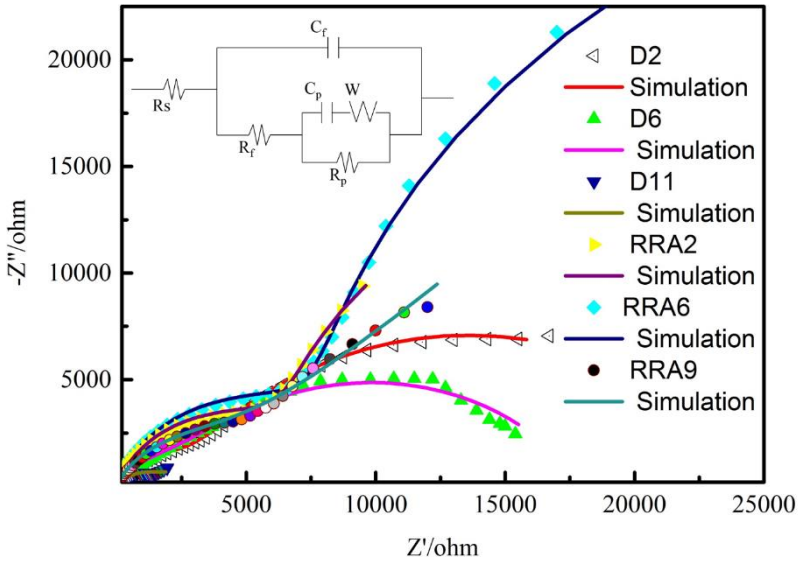

Fig.6. Impedance spectrum pictures and the equivalent circuit diagram

Table.6 The electrochemical impedance data of its equivalent circuit elements

Elements	D2	D6	D11	RRA2	RRA6	RRA9
Rs(Ωcm2)	28.11	10	32.74	28.73	28.09	26.9
Rf (Ωcm2)	3616	49.85	121.2	8760	10410	7241

Preprints (www.preprints.org) | NOT PEER-REVIEWED | Posted: 9 July 2020 doi:10.20944/preprints202007.0173.v1

Rp (Ωcm2)	2.107 E4	2.573 E4	2098	2.838 E4	4.775 E4	2018 E4
C f (μF/cm2)	2.315E-5	8.166 E-5	1.474 E-5	1.818 E-5	1.474 E-5	2.396 E-5
n	0.803	0.4447	0.5424	0.8347	0.8433	0.7824
Cp(μF/cm2)	1.546 E-4	4.438 E-4	3.489 E-4	1.158 E-4	8.929 E-5	1.554 E-4
n	0.714	0.9341	0.8704	1	0.9993	0.8745
W(S-sec^5/ cm2)	2.313 E5	634.1	0.007848	2.486E4	1.4685E4	1.252E6

4. Discussion

4.1 Electron backscattered diffraction

The average grain size was measured from EBSD grain-boundary photograph (Figure 7). It can be seen that the samples treated by T6 or RRA treatment have similar average grain size. The nature of the grain boundaries in the alloy is illustrated in Fig.8 by means of the disorientation distribution histogram. The disorientation distribution histogram was made from EBSD grain-boundary photograph taking into account boundaries with misorientations more than 2 deg. Low angle grain boundaries (LAGB) in 7055 alloy refers to the grain boundary where the misorientations of two adjacent grains are less than 15°. High angle grain boundaries (HAGB) in 7055 alloy refers to the grain boundary where the misorientations of two adjacent grains are more than 15°. The high grain boundary energy leads to the instability of grain boundary, and the mobility on grain boundary also increases. The LAGBs have lower energy than the HAGBs, so the mobility of LAGBs is also higher than that of HAGBs. It can be seen that the percentage of the LAGBs after T6 treatment is 32.461 %, the percentage of the HAGBs after RRA treatment is 42.893%, so the grain boundary mobility of the T6 samples is higher than that of the RRA samples, and the T6 samples are easy to generate continuous distributed high density precipitates on GBs, which offers a path for inter-granular corrosion, the instability grain boundaries with high energy are very sensitive to the corrosion.

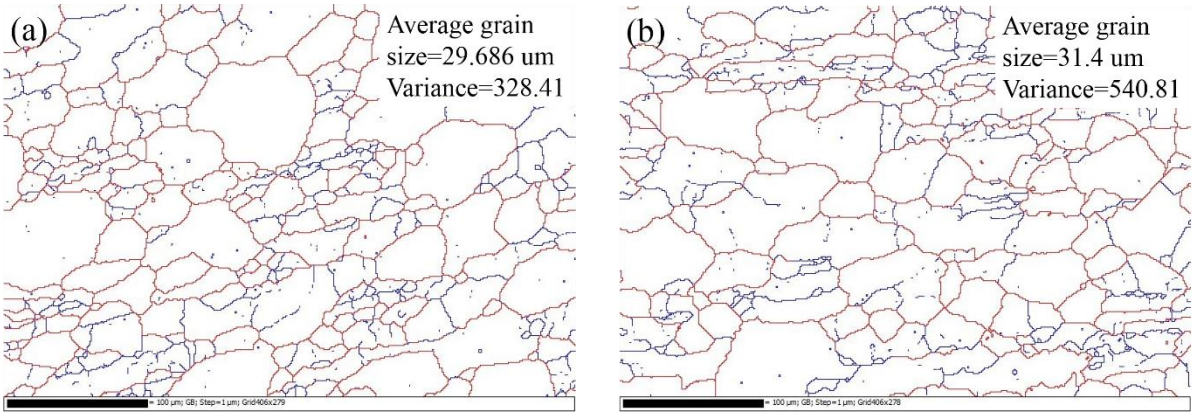

Fig.7. Grain-boundary photograph of (a) the T6 sample; (b) the RRA sample

Preprints (www.preprints.org) | NOT PEER-REVIEWED | Posted: 9 July 2020 doi:10.20944/preprints202007.0173.v1

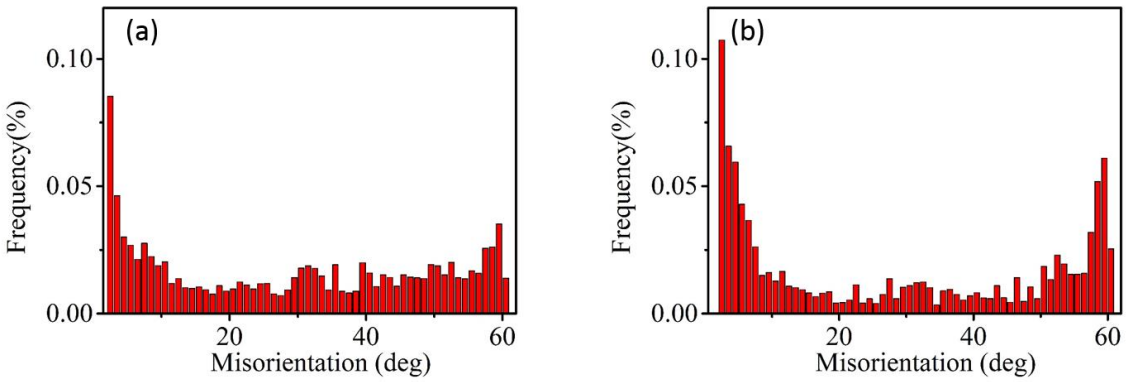

Fig.8. Grain-boundary nature of (a) the T6 sample; (b) the RRA sample

4.2 Microstructure

The precipitates of samples were studied using the TEM observation. The typical bright field TEM micrographs and the selected area diffractions of the 7055 alloy under different aging treatments were shown in Fig.9. In T6 treatment samples, TEM revealed a high density of fine precipitates dispersed relatively uniformly throughout the matrix (Fig.9 (b)). The T6 samples have many η` phases , η phases and some G.P zones in the matrix (Fig.9 (b)), however the RRA samples have many η` phases and η phases in the matrix (Fig.9 (d)). The T6 samples have finer precipitates than the RRA samples, so the T6 samples show better mechanical properties than the RRA samples.

The XRD pattern of the samples treated by different heat treatment parameters is presented in Fig. 10. The precipitated phases can be detected under single-stage aging D11 and retrogression re-aging RRA 9 treatment, they could help to the precipitation strengthening, but they also plays the role of anodic compared with the matrix, so it increase the corrosion or hydrogen embrittlement tendency of the alloy [18]. Moreover, many researchers have confirmed that grain size and orientation, grain boundary precipitation and dislocation have effects on the corrosion of aluminum alloy [19]. The precipitated phases have lower Ecorr, and it has higher Icorr than the phases of matrix [20]. This attributes to the decreasing of corrosion resistance.

The samples under T6 and RRA treatment have different precipitation distribution. A high density precipitated phases are continuous distributed along the GBs under T6 treatment (Fig. 9 (a)). Under RRA treatment (Fig. 9(c)), the precipitates distributed discontinuously and isolated on the GBs, the sizes of which were larger than that of T6 treatment. Under T6 treatment, continuous distributed high density precipitated phases on GBs facilitates the main corrosion path effectively. As for the RRA samples, the isolated precipitates on GBs can interrupt the continuity (Fig. 9(c)), the susceptibility to corrosion of RRA is eliminated or reduced.

Preprints (www.preprints.org) | NOT PEER-REVIEWED | Posted: 9 July 2020 doi:10.20944/preprints202007.0173.v1

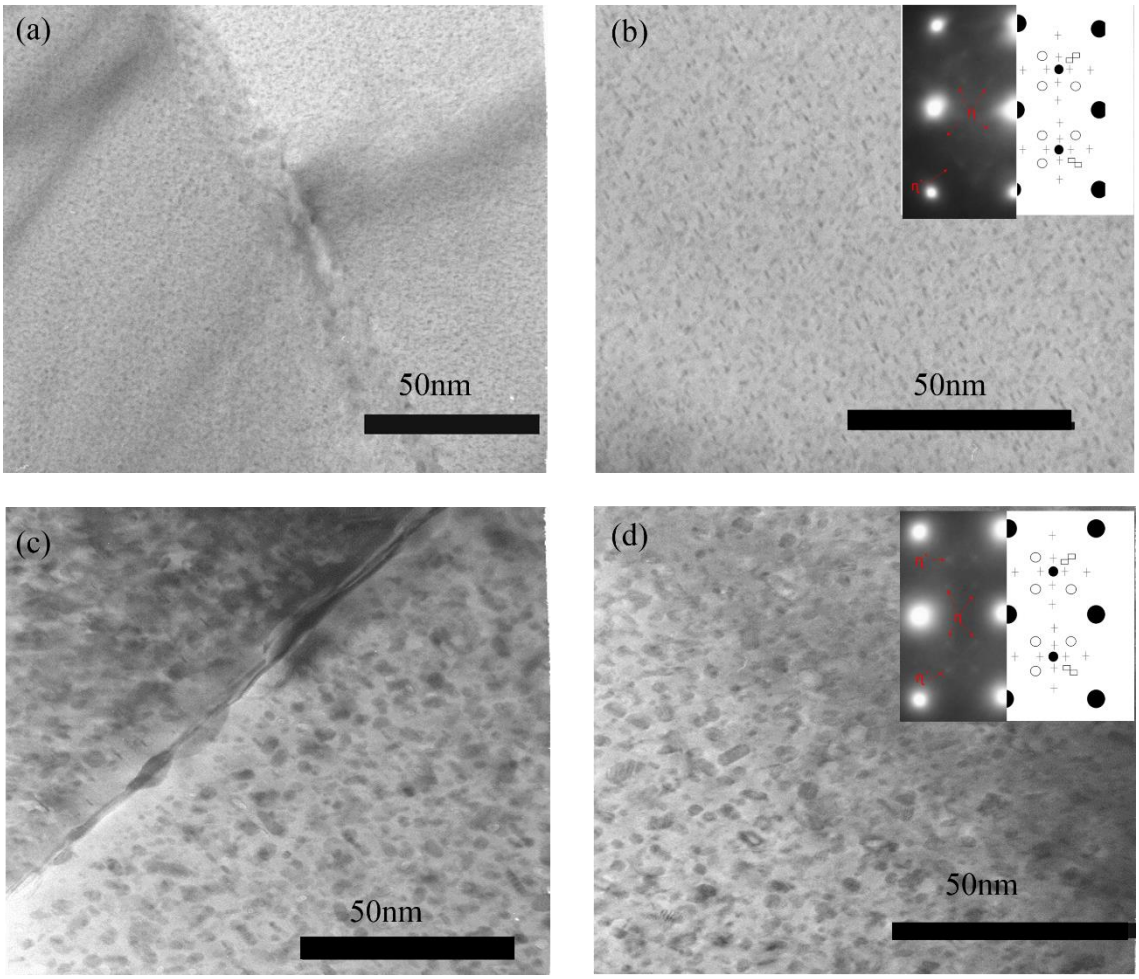

Fig.9. TEM images of the 7055 alloy under different aging treatments: (a), (b) of T6; (c), (d) of RRA.

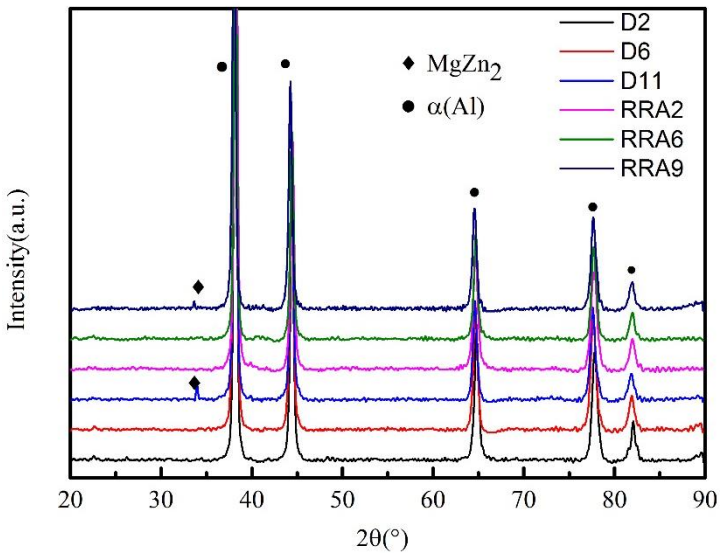

Fig.10. XRD pattern of the samples with different heat treatments.

5. Conclusions

1) The corrosion current density of the RRA 6 (120°C/8h + 190°C/2h +240°C/24h) treatment samples is ten times less than the single-stage peak aging samples with the hardness losing 10%.

2) The corrosion products are generated by the anode branches to form a stagnant layer in corrosion process, and the stagnant layer exhibits Weber impedance. The samples after retrogression re-aging treatment have high Rf, Rp values and low Cf , Cp values, so RRA samples show better corrosion resistance than T6 samples

3) The RRA samples showed the isolated precipitates on GBs and have more contents of the LAGBs than the T6 samples, so the susceptibility to corrosion of RRA samples is reduced.

Author Contributions: Formal analysis, Tao Wang and Yong Zou; Resources, Yong Zou; Software, Fuqiang GUO and Dongting WU; Writing – original draft, Fuqiang GUO; Writing – review & editing, Fuqiang GUO, Shuwei DUAN, Kenji Matsuda, Tao Wang and Yong Zou.

Funding: This research received no external funding.

Acknowledgements: This project is supported by 2018 Key Research and Development Project of Shandong Province (2018CXGC0403).

Conflicts of Interest: We declare that we have no financial and personal relationships with other people or organizations that can inappropriately influence our work. There is no professional or other personal interest of any nature or kind in any product, service or company that could be construed as influencing the position presented in, or the review of the manuscript.

References

1. Sokoluk, M.; Cao, C.; Pan, S.; Li, X., Nanoparticle-enabled phase control for arc welding of unweldable aluminum alloy 7075. *Nature communications* **2019,** 10, (1), 98.
2. Ozer, G.; Karaaslan, A., Properties of AA7075 aluminum alloy in aging and retrogression and reaging process. *Transactions of Nonferrous Metals Society of China* **2017,** 27, (11), 2357-2362.
3. A. Deschamps , Y. B. c., Influence of quench and heating rates on the ageing response of an Al–Zn–Mg–(Zr) alloy. *Materials Science and Engineering A251 (1998) 200–207* **1998**.
4. Oliveira, A. F.; de Barros, M. C.; Cardoso, K. R.; Travessa, D. N., The effect of RRA on the strength and SCC resistance on AA7050 and AA7150 aluminium alloys. *Materials Science and Engineering: A* **2004,** 379, (1-2), 321-326.
5. Xu, D. K.; Birbilis, N.; Rometsch, P. A., The effect of pre-ageing temperature and retrogression heating rate on the strength and corrosion behaviour of AA7150. *Corrosion Science* **2012,** 54, 17-25.
6. Chen, K.; Liu, H.; Zhang, Z.; Li, S.; Todd, R. I., The improvement of constituent dissolution and mechanical properties of 7055 aluminum alloy by stepped heat treatments. *Journal of Materials Processing Technology* **2003,** 142, (1), 190-196.
7. Lin, Y. C.; Jiang, Y.-Q.; Chen, X.-M.; Wen, D.-X.; Zhou, H.-M., Effect of creep-aging on precipitates of 7075 aluminum alloy. *Materials Science and Engineering: A* **2013,** 588, 347-356.
8. Lin, J.-C.; Liao, H.-L.; Jehng, W.-D.; Chang, C.-H.; Lee, S.-L., Effect of heat treatments on the tensile strength and SCC-resistance of AA7050 in an alkaline saline solution. *Corrosion Science* **2006,** 48, (10), 3139-3156.
9. Zhang, J.; Li, J.; Tian, S.; Lv, D., Effects of Solution Treatment on Microstructure Transformation, Tensile and Exfoliation Corrosion Properties of 7136 Aluminum Alloy. *Journal of Materials Engineering and Performance* **2019,** 28, (3), 1312-1323.
10. El-Amoush, A. S., Intergranular corrosion behavior of the 7075-T6 aluminum alloy under different annealing conditions. *Materials Chemistry and Physics* **2011,** 126, (3), 607-613.
11. Huang, T.-S.; Frankel, G. S., Influence of grain structure on anisotropic localised corrosion kinetics of AA7xxx-T6 alloys. *Corrosion Engineering, Science and Technology* **2013,** 41, (3), 192-199.

12. Liu, Y.; Pan, Q.; Li, H.; Huang, Z.; Ye, J.; Li, M., Revealing the evolution of microstructure, mechanical property and corrosion behavior of 7A46 aluminum alloy with different ageing treatment. *Journal of Alloys and Compounds* **2019,** 792, 32-45.
13. Liu, L. L.; Pan, Q. L.; Wang, X. D.; Xiong, S. W., The effects of aging treatments on mechanical property and corrosion behavior of spray formed 7055 aluminium alloy. *Journal of Alloys and Compounds* **2018,** 735, 261-276.
14. Gopala Krishna, K.; Sivaprasad, K.; Sankara Narayanan, T. S. N.; Hari Kumar, K. C., Localized corrosion of an ultrafine grained Al–4Zn–2Mg alloy produced by cryorolling. *Corrosion Science* **2012,** 60, 82-89.
15. Xiao, Y.-P.; Pan, Q.-L.; Li, W.-B.; Liu, X.-Y.; He, Y.-B., Influence of retrogression and re-aging treatment on corrosion behaviour of an Al–Zn–Mg–Cu alloy. *Materials & Design* **2011,** 32, (4), 2149-2156.
16. Chen, S.; Chen, K.; Peng, G.; Jia, L.; Dong, P., Effect of heat treatment on strength, exfoliation corrosion and electrochemical behavior of 7085 aluminum alloy. *Materials & Design* **2012,** 35, 93-98.
17. Zhou, K.; Wang, B.; Zhao, Y.; Liu, J., Corrosion and electrochemical behaviors of 7A09 Al–Zn–Mg–Cu alloy in chloride aqueous solution. *Transactions of Nonferrous Metals Society of China* **2015,** 25, (8), 2509-2515.
18. Stannard, T. J.; Williams, J. J.; Singh, S. S.; Sundaram Singaravelu, A. S.; Xiao, X.; Chawla, N., 3D time-resolved observations of corrosion and corrosion-fatigue crack initiation and growth in peak-aged Al 7075 using synchrotron X-ray tomography. *Corrosion Science* **2018,** 138, 340-352.
19. Rao, A. C. U.; Vasu, V.; Govindaraju, M.; Srinadh, K. V. S., Stress corrosion cracking behaviour of 7xxx aluminum alloys: A literature review. *Transactions of Nonferrous Metals Society of China* **2016,** 26, (6), 1447-1471.
20. Huang, L.; Chen, K.; Li, S., Influence of grain-boundary pre-precipitation and corrosion characteristics of inter-granular phases on corrosion behaviors of an Al–Zn–Mg–Cu alloy. *Materials Science and Engineering: B* **2012,** 177, (11), 862-868.